Creation and Detection of Vector Vortex Modes for Classical and Quantum Communication

Bienvenu Ndagano, Isaac Nape, Mitchell A. Cox, Carmelo Rosales-Guzman, and Andrew Forbes

(Invited Paper)

***Abstract*—Vector vortex beams are structured states of light that are nonseparable in their polarisation and spatial mode, they are eigenmodes of free-space and many fiber systems, and have the capacity to be used as information carriers for both classical and quantum communication. Here, we outline recent progress in our understanding of these modes, from their creation to their characterization and detection. We then use these tools to study their propagation behavior in free-space and optical fiber and show that modal cross-talk results in a decay of vector states into separable scalar modes, with a concomitant loss of information. We present a comparison between probabilistic and deterministic detection schemes showing that the former, while ubiquitous, negates the very benefit of increased dimensionality in quantum communication while reducing signal in classical communication links. This work provides a useful introduction to the field as well as presenting new findings and perspectives to advance it further.**

***Index Terms*—Classical communication, geometric phase, mode division multiplexing, quantum communication, vector vortex modes.**

I. Introduction

STRUCTURED or complex light fields have become highly topical of late, particularly as a means to exploit light's space degree of freedom in optical communication in both the classical and quantum regimes [1]–[3]. This has been fuelled partly by the demand for increased bandwidth and security in communication systems, as well as by the recent advances in the ease of creation and measurement of such structured light fields [4], [5].

Employing spatial modes of light for classical communications channels has been mooted as a future technology, namely mode division multiplexing (MDM) [6], despite having been proposed more than three decades ago [7]. In MDM each spatial mode forms an orthornormal basis, each of which can be used as an independent communication channel upon which classical information encoding can be realised. In seminal work more than a decade ago down the corridors of the University of Glasgow, modes carrying orbital angular momentum (OAM) have been used in a communication link [8], and have subsequently shown, in conjunction with existing multiplexing techniques [9], considerable improvements in data transfer in classical communication systems [1], [2], [10]–[19].

At the single photon level, the use of polarization encoded qubits has become ubiquitous in quantum communication protocols [20]–[23]. Most notably, they have enabled unconditionally secure cryptography protocols through quantum key distribution (QKD) over appreciable distances [24]–[27]. With the increasing technological prowess in the field, faster and efficient key generation together with robustness to third party attacks have become paramount issues to address. A topical approach to overcome these hurdles is through higher-dimensional QKD: increasing the dimensionality, d, of a QKD protocol leads to better security and higher secure key rates, with each photon carrying up to $\log_2(d)$ bits of information [28]–[30]. In this regard, spatial modes carrying OAM have been used in laboratory demonstrations to show increase in photon capacity beyond what is achievable with polarisation encoded qubits, pushing the dimension to as high as $d = 7$ [31]–[33]. The list of reports on high dimensional QKD with spatial modes is not exhaustive as realizing high-dimensional quantum communication remains challenging [34]–[37].

A particular type of structured light takes a so called 'vector form', with spatially non-homogenous polarisation distributions, combining two well-known degrees of freedom: polarisation and spatial mode. In this form of structured light, the spatial and polarization degrees of freedom (DoFs) are coupled in a non-separable manner, reminiscent of entanglement in quantum mechanics [38]. These spatial modes are commonly known as vector modes [39] and have been used as information carriers classically in free-space [40]–[45], but not yet in fibre except for proof-of-principle tests [46], [47]. In the quantum regime, vector modes have been exploited as a new basis [36], [37] and as carriers for polarisation encoded qubits in alignment-free QKD [48], [49]: vector modes that carry OAM, also known as vector vortex modes, exhibit rotational symmetry, removing the need to align the detectors in order to reconcile the encoding and decoding bases, as would be the case in QKD with only polarization.

Here we present an overview of the state-of-the-art techniques for the generation, propagation and detection of vector vortex

Manuscript received August 28, 2017; revised October 18, 2017; accepted October 19, 2017. Date of publication October 25, 2017; date of current version February 24, 2018. *(Corresponding author: Andrew Forbes.)*

B. Ndagano, I. Nape, C. Rosales-Guzman, and A. Forbes are with the School of Physics, University of the Witwatersrand, Wits 2050, South Africa (e-mail: nibienvenu@gmail.com; isaacnape@gmail.com; carmelo.rosalesguzman@wits.ac.za; Andrew.Forbes@wits.ac.za).

M. A. Cox is with the School of Electrical Engineering, University of the Witwatersrand, Wits 2050, South Africa (e-mail: mitch@enox.co.za).

Color versions of one or more of the figures in this paper are available online at http://ieeexplore.ieee.org.

Digital Object Identifier 10.1109/JLT.2017.2766760

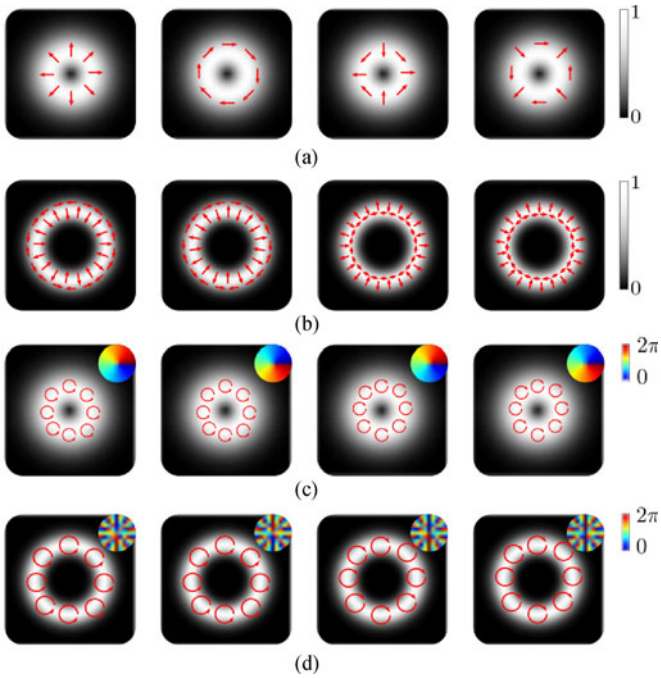

Fig. 1. Vector vortex modes with (a) $\ell = \pm 1$ and (b) $\ell = \pm 10$, and their corresponding OAM scalar modes with (c) $\ell = \pm 1$ and (d) $\ell = \pm 10$. The insets show the phase profile of the scalar OAM modes.

modes. Using a toolkit borrowed from the quantum world, we show that entanglement measures can be used to describe such beams in a quantitative manner. We show how they can be detected by either a filter based approach or a deterministic approach, and highlight the impact this choice has on both classical and quantum communication channels. Using these tools we present results on the propagation of vector vortex modes through perturbing media, namely, free-space with atmospheric turbulence and optical fibre with modal cross-talk.

II. Basic Definitions

Both scalar and vector OAM modes form orthogonal bases with which to describe spatial modes of light, with one a linear combination of the other. To expand on this statement, consider an electric field $\mathbf{E}$ expressed in polar coordinates $\mathbf{r} = (r, \phi)$, as follows:

$$\mathbf{E} = \cos(\theta)\exp(i\ell\phi)\hat{R} + \sin(\theta)\exp(-i\ell\phi + i\gamma)\hat{L}, \qquad (1)$$

where γ is the intra-modal phase, θ parametrizes the amplitudes of the right- and left-circular polarisation states, respectively, labelled as $\hat{R}$ and $\hat{L}$. The functions $\exp(i\ell\phi)$ are OAM eigenfunctions of integer topological charge ℓ. By tuning the parameter θ, one controls the nature of the spatial mode in Eq. (1). In the instance where $\theta = \pi/4$ one obtains all vector vortex modes shown in Fig. 1(a) and (b) for $\ell = \pm 1$ and $\ell = \pm 10$, respectively. Similarly, by setting $\theta = 0$ or π, one can produce either a right- or left- circularly polarised scalar OAM beam, respectively, as shown in Fig. 1(c) and (d).

It is also evident that vector modes have intertwined degrees of freedom, spatial and polarisation, in a non-separable fashion; that is, the polarisation, as well as the electric field

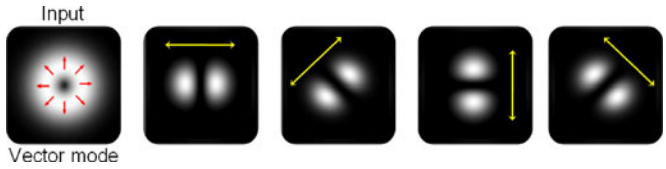

Fig. 2. An input vector mode is passed through a linear polariser whose axis is shown by the yellow arrows in the figures.

distribution, vary across the transverse plane (see Fig. 1). A qualitative demonstration of this relation between the polarisation and spatial DoFs is graphically depicted in Fig. 2. An input vector mode is passed through a linear polariser and the intensity measured is recorded. Observe that the two-lobe pattern obtained rotates together with the transmission axis of the polariser, indicated by the yellow arrows. One deduces that the polarisation measurement performed on a vector vortex beam, determines the spatial distribution pattern obtained, hence the non-separability.

Vector modes have long been known to be eigenmodes of optical fibres, referred to as waveguide modes. More recently, Milione *et al.* have shown that such states of light may be described by positions on a High-order Poincaré sphere (HOPS) [50] that describes the total angular momentum of light, as an analogy to the familiar Poincaré sphere that contains only the spin angular momentum component [51]. In this pictorial representation, vector modes are mapped to points on a sphere where, the poles are circularly polarised OAM scalar modes and the equator represents the set of well-known cylindrical vector vortex beams [39]. More than a representation, the HOPS summarises the basic recipe of how vector modes can be generated: a weighted superposition of basis scalar modes, marked with orthogonal polarisation, as given in (1), for all vector vortex modes.

Note that in general the spatial modes would have amplitude terms as well as phase terms associated with each polarisation component. These are spatial enveloping functions that determine the electric field distribution of the vector vortex mode. For example, the intensity profiles shown in Fig. 1 clearly have donut profiles, which requires a radial term to the amplitude. One could adapt (1) to reflect this as follows:

$$\mathbf{E} = A_\ell(r,\phi)\left(\exp(i\ell\phi)\hat{R} + \exp(-i\ell\phi + i\gamma)\hat{L}\right), \qquad (2)$$

where we have dropped the weighting terms for clarity. Here $A_\ell(r,\phi)$ reflects the enveloping amplitudes (for the two signs of ℓ, both having the same function). For example, they can be tailored to produce vector OAM Bessel beams [52], or the amplitude terms required for step-index fibre [46] and free-space [53] propagation. The amplitude envelop is, however, often factored out of the mathematical expression of vector beams (and scalar OAM modes) because it is common to use the OAM component as the information carrier. This is because this component can be detected in a phase-only manner, in principle without any loss, whereas detecting the amplitude terms necessarily requires complex amplitude modulation: more complicated and/or lossy (with two elements it can be lossless while with one it is always lossy). It is thus common to ignore the radial and azimuthal

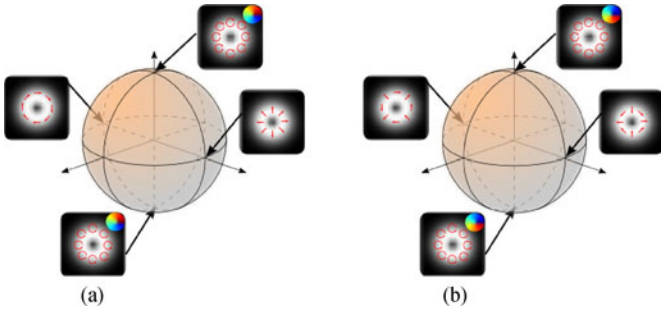

Fig. 3. On the higher order Poincaré sphere, the poles represent the basis scalar modes from which the vector modes, located on the equator, are constructed. This is shown for basis circularly polarised OAM modes with (a) $\ell = 1$ and $\ell = -1$.

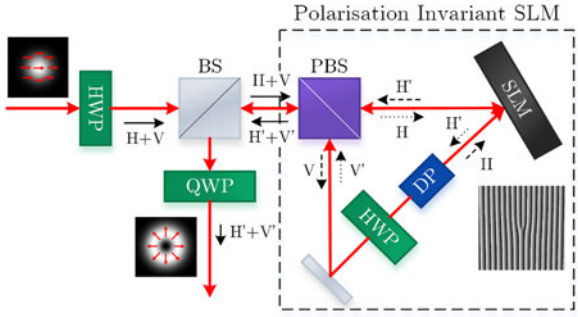

Fig. 4. An incident polarised laser beam is spatially divided in horizontal and vertical polarisation components using a polarising beam splitter (PBS), each of which is modulated by a single hologram encoded on an SLM, placed inside a Sagnac interferometer. The dove prism (DP) ensured that the two OAM modes produced have opposite charge ℓ. BS: 50:50 beam splitter; HWP: half-wave plate; QWP: quarter-wave plate. H, H', V and V' denote the polarisation paths before and after the SLM.

amplitude function when describing vector vortex beams. The vector field expressed in (1) is however not a solution of free-space. Consequently such fields result in the excitation of additional radial eigenmodes of the medium in which they are propagating, manifesting in the excitation of undesired radial modes with a large energy component [54].

Recently it has become commonplace to formulate the above in a quantum language, reflecting the fact that such modes of light are non-separable in their two degrees of freedom, akin to quantum entanglement. This so-called classical entanglement [55]–[61] is highly controversial but has also found some practical advantages over separable (scalar) states of light [34], [62]–[67]. Using Dirac's notation, we can denote a four dimensional space spanned by four scalar OAM modes, $\{|\ell, L\rangle, |-\ell, L\rangle, |\ell, R\rangle, |-\ell, R\rangle\}$, to form the cylindrical vector vortex modes as

$$|\mathrm{TM}\rangle = \frac{1}{\sqrt{2}}(|\ell, R\rangle + |-\ell, L\rangle), \tag{3}$$

$$|\mathrm{TE}\rangle = \frac{-i}{\sqrt{2}}(|\ell, R\rangle - |-\ell, L\rangle), \tag{4}$$

$$|\mathrm{HE}\rangle_e = \frac{1}{\sqrt{2}}(|\ell, L\rangle + |-\ell, R\rangle), \tag{5}$$

$$|\mathrm{HE}\rangle_o = \frac{i}{\sqrt{2}}(|\ell, L\rangle - |-\ell, R\rangle), \tag{6}$$

The interest in these vector states as a basis for information transfer resides in the fact that there are an infinite number of such four dimensional spaces, one for each value of $|\ell|$, i.e., an infinite number of HOPS to exploit. For each HOPS we can assign the elements 00, 01, 10, and 11 to the TE, TM, HE_e and HE_o modes as our information carriers. Fortunately, the means to create and detect such states on the HOPS have also recently been developed.

III. Generation of Vector Vortex Modes

Vector vortex beams have long been created internal to lasers by exploiting gain competition in birefringent laser crystals [68] and more recently with geometric phase [69] and with structured materials in on-chip solutions [70]–[74]. While we acknowledge that such custom solutions exist, they are not common to most laboratories. Here we consider more standard and accessible approaches to the creation of such modes.

From (1), one deduces that in order to generate a vector beam though dynamic phase (optical path length) manipulation requires a device that can independently modulate the two polarisation components. This can be achieved using a spatial light modulator (SLM); the liquid crystals present in the display of an SLM can be individually addressed in order to spatially control the refractive index distribution of the digital hologram used to modulate the incident beam (see Refs. [5] for a comprehensive review on beam shaping with SLMs). The birefringent liquid crystals only allow phase modulation of one polarisation component and so special tricks are needed to overcome this for vector beam generation with SLMs [4] and digital micromirrors [75], [76].

Early use of SLMs to tailor vector vortex beams involved placing them inside an interferometer, as first demonstrated by Neil *et al.* [77]. By splitting the beam into orthogonal polarisations, one can align the polarisation axes of the two beams to match the SLM and independently modulate the two beams before recombination at a later stage, as shown in Fig. 4. Due to the difference in the number of reflections, each polarisation component acquires oppositely OAM values. This approach was later generalised in [78]. Other variants of the generation of vector modes with SLMs involve a double pass on each of the two different hologram [79]. In between each pass, the polarisation is rotated to allow modulation of only one polarisation component.

A novel approach to beam shaping of vector beams makes use of geometric phase rather than dynamic phase. First introduced by Pancharatnam and later generalized by Berry, the geometric phase naturally arises when a system in an initial state on a sphere is moved along a closed path back to its initial position [80], [81]. Galvez *et al.* have shown that the same geometric phase also arises from similar transformations on the OAM Bloch sphere [51], [82].

The geometric phase equally arises as a result of birefringence. As a beam propagates through an anisotropic medium,

TABLE I
GENERATION OF SCALAR AND VECTOR VORTEX MODES THROUGH GEOMETRIC PHASE CONTROL USING A q-PLATE

Input polarisation	q-plate charge	output mode
$\hat{R}$	1/2	$\exp(-i\phi)\hat{L}$
$\hat{L}$	1/2	$\exp(i\phi)\hat{R}$
$\hat{R}$	-1/2	$\exp(i\phi)\hat{L}$
$\hat{L}$	-1/2	$\exp(-i\phi)\hat{R}$
$\hat{H}$	1/2	TM $(\ell = 1)$
$\hat{V}$	1/2	TE $(\ell = 1)$
$\hat{H}$	-1/2	HE_e $(\ell = 1)$
$\hat{V}$	-1/2	HE_o $(\ell = 1)$

The input mode in all cases is a Gaussian beam with OAM charge $\ell = 0$.

the orthogonal polarisation states experience different refractive indices, resulting in different optical phases on each polarisation state. The nature of the phase acquired depends on the geometry of the birefringence, hence a geometric phase. A recent example of this is the so-called q-plate, which has a locally varying birefringence resulting in spin-orbit coupling [83], [84]. The transformation of a q-plate can be summarised as

$$\exp(i\ell\phi)\hat{L} \xrightarrow{q\text{-plate}} \exp(i(\ell + 2q)\phi)\hat{R} \tag{7}$$

$$\exp(i\ell\phi)\hat{R} \xrightarrow{q\text{-plate}} \exp(i(\ell - 2q)\phi)\hat{L} \tag{8}$$

where q is the charge of the q-plate. By this approach all states shown on the HOPS in Fig. 3 can be produced, as shown in Table I.

It is worth noting that the geometric phase transformation outlined in (7) and (8), have been implemented experimentally using sub-wavelength gratings [85]–[89] and metamaterials [90]–[93]. What remains then is to determine which mode has been produced, and to what purity.

IV. DETECTION OF VECTOR VORTEX BEAMS

The determination of the vectorial nature of an optical field has typically been qualitative or at best through an average degree of polarisation across the field. Due to the spatially variant polarisation map, vector vortex beams produce intensity patterns that vary when passed through a rotating polariser [39], as shown in Fig. 2, and one routinely sees such plots as a confirmation of the vector nature of the light under study. Such a measurement is however not adequate to determine quantitatively the quality of the vector beam produced. Nowadays there are new approaches to quantitatively measure the quality of a vector vortex beam. Before we get into the details of these techniques, it is important to understand their origins.

A. The Vector Quality Factor

The first measure quantifies non-separability. From the expression of a vector beam in (1) we see that depending on the value of θ, the superposition is either non-factorizable or factorizable in terms of the individual degrees of freedom. For example, for $\theta = \pi/4$ the electric field $\mathbf{E}$ cannot be expressed as a product function of the following kind:

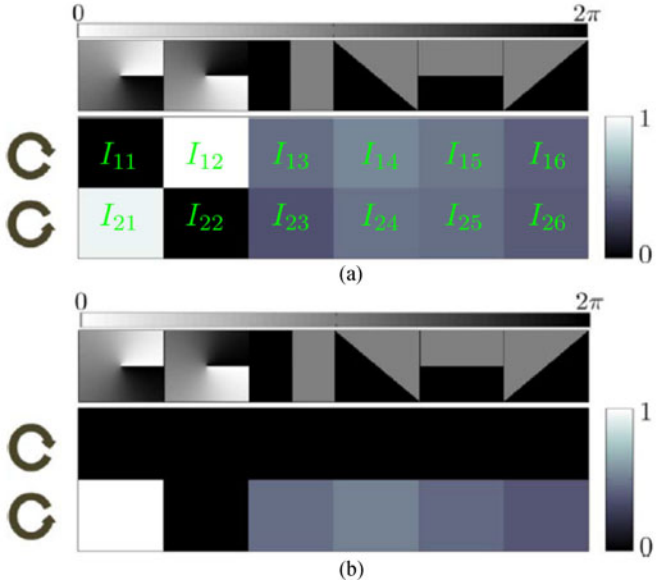

Fig. 5. Normalized projections of the left- and right-circular polarisation states, onto OAM eigenstates of the Pauli matrices for (a) a vector mode and (b) a scalar mode.

$\mathbf{E} = space \times polarisation$. The space and polarisation DoFs are thus said to be non-separable. We can define a new beam quality factor for vector beams, a 'vector quality factor' [38], [94]. The measure finds its origins in the quantum world, where measures of entanglement quantifies non-separability between multi-photon states. Here we use it to define the vector quality by monitoring the non-separability of the state. With respect to a vector mode defined as in (1), the vector quality factor (VQF) is defined as

$$\text{VQF} = \text{Re}\left(\sqrt{1 - s^2}\right) = 2|\cos(\theta)\sin(\theta)|, \tag{9}$$

where s^2 is the length of the Bloch vector, defined with respect to expectation values of the Pauli matrices σ_i:

$$s^2 = \sum_{i=1}^{3} \langle\sigma_i\rangle^2 \tag{10}$$

The expectation values $\langle\sigma_i\rangle$ are obtained by performing an optical projection of the vector beam onto the eigenvectors of the matrices σ_i. There is of course the issue of identifying the DoF in which the projections are realised. Here, the choice is arbitrary; one can either project each OAM eigenmode onto polarisation eigenstate or vice-versa. The latter is preferred as it can be automated using either an SLM or a digital micromirror, allowing for simultaneous measurements of all expectation values through spatial mode demultiplexing [94]. The expectation values $\langle\sigma_i\rangle$ are computed as follows:

$$\langle\sigma_1\rangle = (I_{13} + I_{23}) - (I_{15} + I_{25}), \tag{11}$$

$$\langle\sigma_2\rangle = (I_{14} + I_{24}) - (I_{16} + I_{26}), \tag{12}$$

$$\langle\sigma_3\rangle = (I_{11} + I_{21}) - (I_{12} + I_{22}). \tag{13}$$

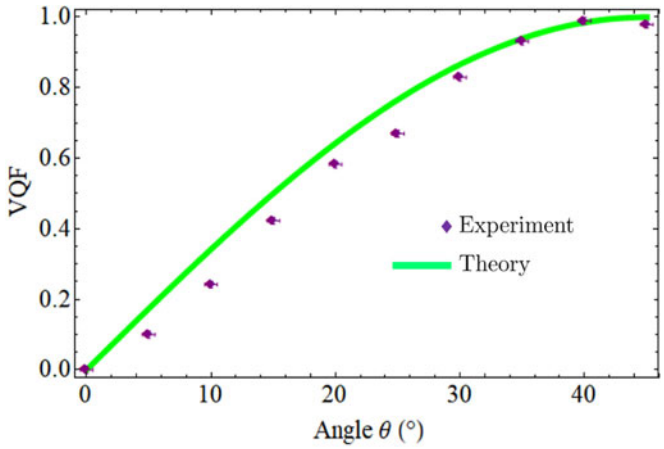

Fig. 6. Experimental and theoretical variation of the VQF with respect to the amplitude parameter θ.

The layout of the projections is shown in Fig. 5. The grayscale images on the top represent the phase holograms encoded on the SLM to realize the spatial projections, six for each of the two polarisations to be measured, so 12 measurements in total.

By measuring the expectation values $\langle \sigma_i \rangle$ as a function of the parameters θ, one obtains a variation of the VQF from 0 to 1 for $0 \leq \theta \leq \pi/4$, as shown on Fig. 6. Note that varying θ from 0 to $\pi/4$ is equivalent to a motion on the HOPS, from the pole to the equator where the vector vortex modes with maximum non-separability are located.

B. Deterministic and Filter-Based Detections

The second quantitative measure of 'vectorness' is the traditional modal decomposition, extensively demonstrated in the case of scalar beams [95]–[98]. It is however useful to go over the technique in the case of vector vortex beam. Note that the following example can be generalised to other forms of vector and scalar modes. The aim of vector modal decomposition is to express an arbitrary optical field $\mathbf{U}$ as a weighted superposition of basis vector modes ψ_ℓ: $\mathbf{U} = \sum_\ell c_\ell \psi_\ell$, where c_ℓ are complex coefficient, appropriately normalized; that is $\sum_\ell |c_\ell|^2 = 1$. in the case where vector vortex modes are used as basis, we can write the basis states ψ_ℓ as follows:

$$\psi_\ell^{\pm} = \frac{1}{\sqrt{2}} \left(\exp(i\ell\phi)\hat{R} \pm \exp(-i\ell\phi)\hat{L} \right). \tag{14}$$

Let $\mathbf{U}$ be a vector vortex mode in this basis that is used to carry a given stream of information. We write $\mathbf{U}$ as follows:

$$\mathbf{U} = \frac{1}{\sqrt{2}} \left(\exp(im\phi)\hat{R} + \exp(-im\phi)\hat{L} \right). \tag{15}$$

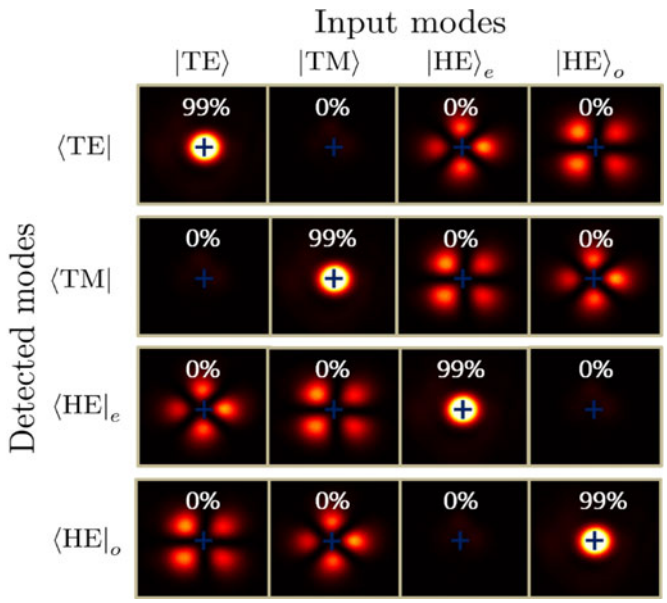

Fig. 7. Experimental Modal decomposition of vector vortex modes in the $\ell = \pm 1$ subspace.

The coefficients $|c_\ell^{\pm}|^2$, can be associated with physical detectors, and are given as follows

$$|c_\ell^{\pm}|^2 = \frac{1}{2\pi} \sum_\ell \left| \int_{\mathbb{R}^2} d\mathbb{R}^2 \; \psi_\ell^{\pm^*} \mathbf{U} \right|^2, \tag{16}$$

$$= \frac{1}{4\pi} \sum_\ell \left| \int_{\mathbb{R}^2} d\mathbb{R}^2 \; e^{i(m-\ell)\phi} \pm e^{-i(m-\ell)\phi} \right|^2, \tag{17}$$

$$= \frac{1}{2} \sum_\ell |\delta_{m,\ell} \pm \delta_{m,\ell}|^2 . \tag{18}$$

One then deduce the following result

$$|c_\ell^{-}|^2 = 0 \text{ and } |c_\ell^{+}|^2 = \begin{cases} 1 \; \ell = m \\ 0 \; \ell \neq m \end{cases}$$

The implication is that only one vector mode detector, among the multitude one can construct in this basis, will register a signal from the transmission on $\mathbf{U}$. A graphical example of such a detection implemented experimentally is shown in Fig. 7. Within a four-dimensional basis set of vector modes with OAM charge $\ell = 1$. each element is decomposed with respect to itself and the others. The cross-talk, that is the amount of power measured in a given mode i for an input mode j, is numerically shown for each input mode.

This vector mode decomposition was first introduced by Milione *et al.* in the context of classical vector mode multiplexing in free-space [43]. As depicted in Fig. 8(a) a vector beam generated with geometric phase optics is set along two paths. In each of the paths, a q-plate, together with a polarising beam splitter act as a filter for vector modes. This method however comes with an inherent 50% loss in intensity (photon number). Note that the two arms contain slightly different filters: one has a half-wave plate while the other does not. It can be shown by matrix algebra that the half-wave plate changes the sign of the

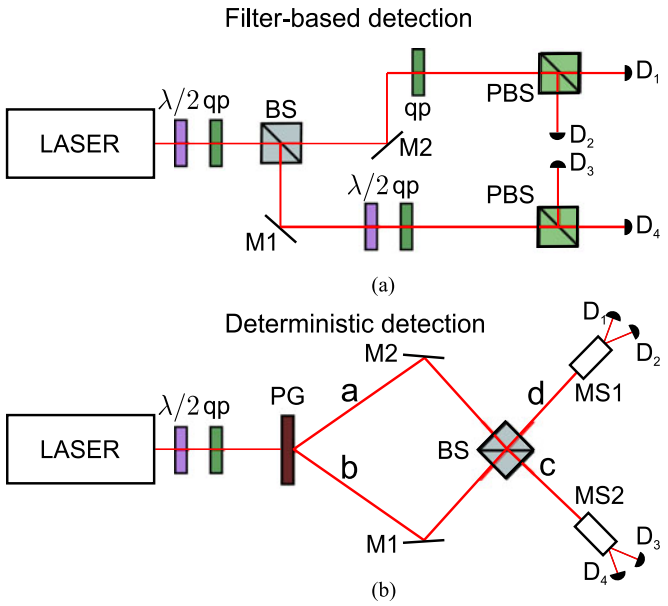

Fig. 8. A vector vortex beam is generated by transforming a linearly polarised Gaussian laser beam with a half-wave plate and a q-plate. (a) The vector beam is sent along two paths, each having a vector mode filter based on geometric phase. (b) The generated vector beam is passed through a Mach-Zehnder interferometer that resolves intra-modal phases. The two outputs of the interferometer are sent to OAM mode sorters that resolves the OAM content.

charge of the q-plate. The implication is that each arm is set to only detect a maximum of two vector vortex modes, the other two giving identical signals. At the classical level, demultiplexing vector modes shown in Fig. 3 using the setup in Fig. 8(a) would result in lower signal-to-noise ratio due to the 50% loss at the beam-splitter. In the context of quantum key distribution, such a loss would result in lower sifting and effective key rates, negating the benefit of the higher-dimensional space provided by spatial modes. One can overcome this by exploiting interference of modes, and this has been done in a manner where the OAM subspace is predetermined and fixed [44]. It is in light of this that we introduce a novel method based on mode-to-space mapping that works for any OAM subspace; that is, any spatial mode is mapped to a set of spatial coordinate with, in principle, unit probability [36].

Consider a vector mode defined as follows

$$\mathbf{E} = \frac{1}{\sqrt{2}}\left(\exp(i\ell\phi)\hat{R} + \exp(-i\ell\phi + i\gamma)\hat{L}\right). \tag{19}$$

The sorting of the different vector modes is achieved through a combination of geometric phase control and multi-path interference as shown in Fig. 8(b). First, a polarisation grating based on geometric phase [99] acts as a beam splitter for left- and right-circularly polarised photons, creating two paths

$$\mathbf{E} = \frac{1}{\sqrt{2}}\left(\exp(i\ell\phi)\hat{R}_a + \exp(-i\ell\phi + i\gamma)\hat{L}_b\right), \tag{20}$$

where the subscript a and b refer to the polarisation-marked paths. The photon paths a and b are interfered at a 50:50 BS. The optical phase difference between the path is set to $\pi/2$,

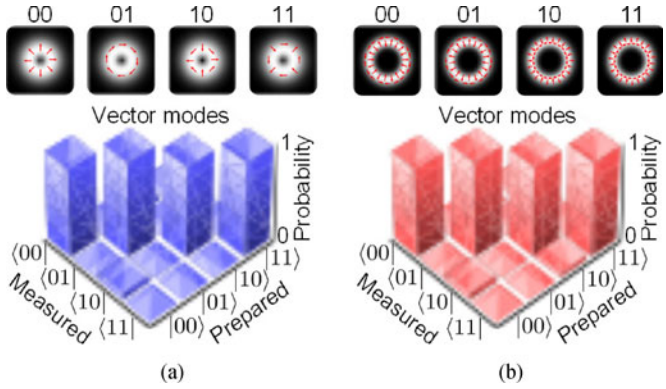

Fig. 9. Crosstalk measurement for vector modes in the subspaces (a) $\ell = \pm 1$ and (b) $\ell = \pm 10$.

resulting in the following state after the BS:

$$\mathbf{E}' = \left(\frac{1 - e^{i\gamma}}{2}\right)\exp(i\ell\phi)_c + i\left(\frac{1 + e^{i\gamma}}{2}\right)\exp(-i\ell\phi)_d. \tag{21}$$

where the indices c and d label the output ports of the BS. Note that the polarisation of the two paths is automatically reconciled in each of the output ports of the beam splitter due to the difference of parity in the number of reflections for each input arm. Hence, we drop the polarisation vectors in each output arm. Also note that at this point it is not necessary to retain the polarisation kets in the expression of the photon state since the polarisation information is contained in the path. The measurement system is completed by passing each of the outputs in c and d through a mode sorter and collecting the photons using 4 fibres coupled to avalanche photodiodes. The mode sorters are refractive (lossless) aspheres that map OAM to position [52], [100]–[102]. The mapping is such that

$$\gamma = 0 \qquad \rightarrow \mathbf{E}' = i\exp(-i\ell\phi)_d, \tag{22}$$

$$\gamma = \pi \qquad \rightarrow \mathbf{E}' = -\exp(i\ell\phi)_c, \tag{23}$$

In each output arm c and d, the OAM mode sorters maps $\pm\ell$ OAM state to distinct spatial positions. In this way, all the vector modes defined as in (19) can be mapped to independent positions, thus achieving a complete sorting of vector modes with unit efficiency. This holds at both the classical and quantum levels. Graphical representation of the cross-talk measured for vector modes of the $|\ell| = 1$ and $|\ell| = 10$ subspaces is shown in Fig. 9.

The advantage of our approach is graphically depicted in Fig. 10(a), where we plot, as a function of the dimension, the photon efficiency of the detection: defined as $1 - S$ where S is the fraction of photons whose information is lost due to measurement approach. Since a filter can only probe one spatial mode at the time, the measurement of a d-dimensional state will return a positive detection with an average probability $\leq 1/d$. In two dimensions, two modes can be detected at once by inferred from the state of a single detectors; given that the probability of a detection in detector A is p_A, the probability of detection in detector B is thus $1 - p_A$.

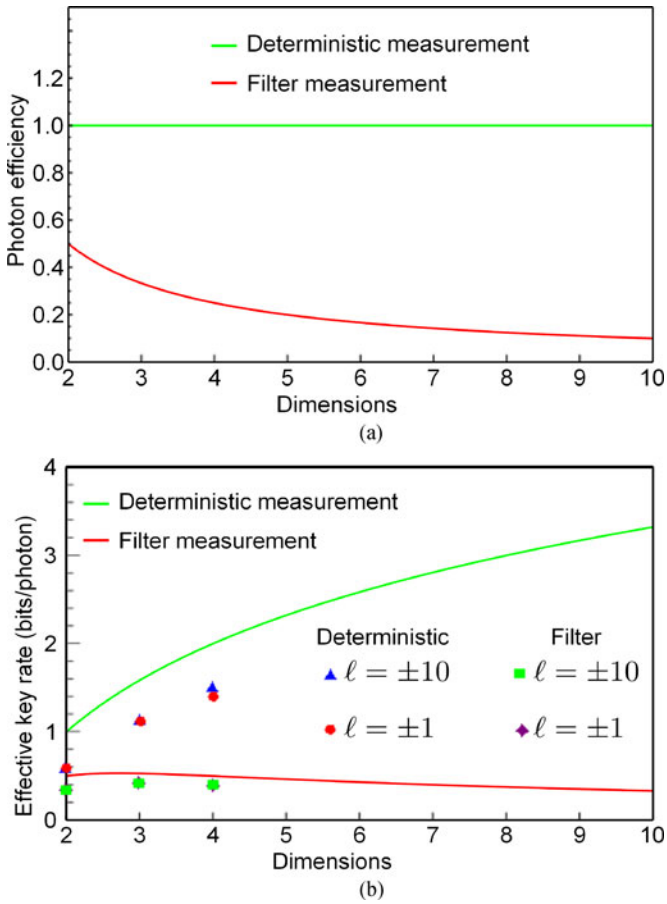

Fig. 10. (a) Photon efficiency as a function of dimension for a deterministic and filter-based measurement scheme. (b) Effective key rate as a function of dimension shown experimentally (data points) for two measurement approaches, namely, filtering and deterministic detection. Data points show measurements in the subspaces of $\ell = \pm 1$ and $\ell = \pm 10$ for $d = 2$,3 and 4. The measurement fidelities for $\ell = \pm 1$ and $\ell = \pm 10$ were measured to be 0.96 and 0.97, respectively. The solid curves are theoretical bounds on the effective key rate assuming a fidelity of 1.

Our system on the other hand does not suffer any dimension dependent loss. This would make it particularly beneficial to both classical communication through mode-division multiplexing with higher signal-to-noise ratio, as well as high efficiency quantum communication in the form of high-dimensional quantum key distribution. The latter is graphically illustrated in Fig. 10(b) where we plotted theoretical and experimental data of the photon information capacity as a function of the dimension. By photon information capacity we mean the d-dimensional effective key rate as defined in [103], taking into account detection efficiency. Note that the filter-based detection has key rates well below the qubit $(d = 2)$ maximum of 1 bit per photon.

V. Propagation Through Perturbing Media

When propagating through various communication channels (free-space and fibres), vector vortex modes are affected by the imperfections of the medium, for example, turbulence in free-space and impurities and stress in optical fibres. This results in intermodal cross-talk and interference which affects the spatial mode of interest. Consider for example the propagation of a radially polarised vector vortex mode through turbulence:

$$\mathbf{E} = \frac{1}{\sqrt{2}}\left(\exp(i\ell\phi)\hat{R} + \exp(-i\ell\phi)\hat{L}\right). \tag{24}$$

The atmosphere is largely non-birefringent. As such, the polarisation is unaffected during propagation. The spatial degree of freedom however is highly susceptible to atmospheric turbulence, causing a scattering among OAM states [104]–[108]. Let us consider vector modes of a given OAM subspace ℓ. After turbulence, the final vector modes state can be expressed as follows

$$\mathbf{E}'(\xi', \xi) = \frac{\cos(\xi)\exp(i\ell\phi) + \sin(\xi)\exp(-i\ell\phi)}{\sqrt{2}}\hat{R} + \frac{\cos(\xi')\exp(-i\ell\phi) + \sin(\xi')\exp(i\ell\phi)}{\sqrt{2}}\hat{L}, \tag{25}$$

where ξ and ξ' parametrize the scattering amplitude between OAM modes in the ℓ subspace, with $0 \leq \xi, \xi' \leq \pi/4$. In the absence of turbulence, $\xi = \xi' = 0$ and one recovers the state in (24). In infinitely strong turbulence, $\xi = \xi' = \pi/4$; that is, all OAM states have equal probability and the information on the initial state is 'erased'. Given the structure of the atmosphere, it can be considered a non-chiral medium; i.e., the $\pm\ell$ OAM eigenstates should experience similar scattering when going during propagation. Thus, it is reasonable to assume $\xi = \xi'$. Borrowing tools from quantum mechanics, the VQF of the state $\mathbf{E}'$ can be expressed in the same fashion as the concurrence for entangled state [109]:

$$\mathrm{VQF}(\mathbf{E}') = |\cos^2(\xi) - \sin^2(\xi)| = |\cos(2\xi)|. \tag{26}$$

For $\xi = 0$, we have $\mathbf{E}'(0) = \mathbf{E}$; that is, in the absence of turbulence, the final state is a pure vector mode with VQF $= 1$. In the case of infinitely strong turbulence, $\xi = \pi/4$ and after some simple algebra, one can show that the final state $\mathbf{E}$' is expressed as follows

$$\mathbf{E}'(\xi) = \frac{1}{\sqrt{2}}\left(\exp(i\ell\phi) + \exp(-i\ell\phi)\right)\left(\hat{R} + \hat{L}\right) = \cos(\ell\phi)\hat{H}, \tag{27}$$

where $\hat{H} = \left(\hat{R} + \hat{L}\right)/\sqrt{2}$ is the horizontal polarisation state. By definition, $\mathbf{E}'(\pi/4)$ is a scalar mode and therefore, a separable state. As such, $\mathrm{VQF}(\mathbf{E}'(\pi/4)) = 0$. A similar analysis holds for optical fibre, where the VQF of modes in a fibre will vary as the modes propagate due to mode coupling.

We can confirm the above analysis experimentally. In Fig. 11(a), we show the cross-talk matrix for a set of vector modes with $|\ell| = 1$, propagating in a non-perturbative medium. We then compare it to Fig. 11(b) which shows the the cross-talk matrix of the same vector modes propagating a 5 cm long step-index optical fibre with core diameter 30 μm, supporting 76 modes at an operating wavelength of 633 nm. Note that in general, one is more likely to measure a vector mode that is different from the one that was injected. This is because of the strong anti-diagonal nature of the cross-talk matrix that characterises the fibre. In Fig. 11(c) and (d), the vector modes are made to propagated in medium and strong atmospheric turbulence conditions, respectively. The measure of turbulence used

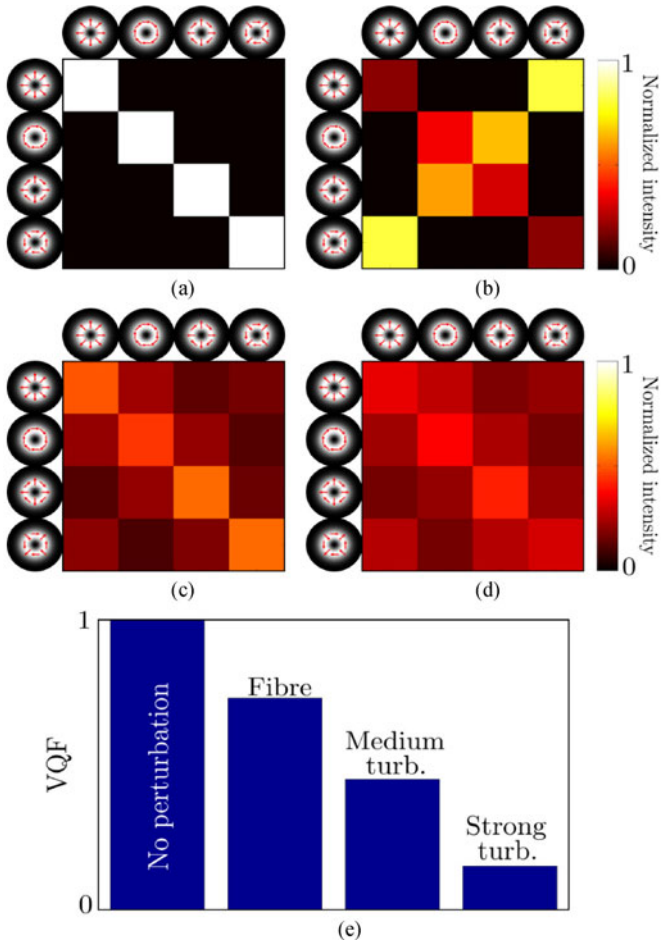

Fig. 11. Crosstalk measurement of vector modes vector vortex modes propagating in (a) unperturbed conditions, (b) step index fibre, atmospheric turbulence at (c) medium ($SR = 0.6$) and (d) strong levels ($SR = 0.2$). (e) As a result we note a decrease in the VQF from the initial ideal conditions.

here is the Strehl Ratio SR [110], ranging from 0 to 1 (0 is for very strong turbulence and 1 for no turbulence). Note that the detection probabilities diminish with increasing turbulence strength. Following the characterisation method of the VQF, we find that as expected the VQF decreases due to the modal coupling, shown in Fig. 11(e). This decrease in VQF with increasing turbulence highlights the lack of resilience of vector vortex modes to atmospheric turbulence [111]. Finally, we point out that while we have used mode coupling in turbulence and fibre as two relevant examples of perturbing media, we do not imply that the underlying physics of the two are the same.

VI. Conclusion

In this work we have briefly reviewed the salient tools for the creation, characterisation and detection of vector vortex beams. We have highlighted their applicability as information carriers in classical and quantum communication, and shown some examples of the degradation of such modes in perturbing media such as free-space with turbulence and imperfect optical fibre. We present a comparison between probabilistic and deterministic detection schemes showing that the former, while ubiquitous, negates the very benefit of increased dimensionality in quantum communication while reducing signal in classical communication links. Our newly proposed deterministic scheme overcomes this limitation. We anticipate that this exciting field is likely to grow rapidly and believe that this work will offer a good starting point for new researchers in the field.

References

[1] A. E. Willner *et al.*, "Optical communications using orbital angular momentum beams," *Adv. Opt. Photon.*, vol. 7, no. 1, pp. 66–106, 2015.
[2] A. E. Willner *et al.*, "Recent advances in high-capacity free-space optical and radio-frequency communications using orbital angular momentum multiplexing," *Philos. Trans. Roy. Soc. A, Math., Phys. Eng. Sci.*, vol. 375, no. 2087, 2017, Art. no. 20150439.
[3] H. Rubinsztein-Dunlop *et al.*, "Roadmap on structured light," *J. Opt.*, vol. 19, Jan. 2017, Art. no. 013001.
[4] C. Rosales-Guzmán and A. Forbes, *How to Shape Light With Spatial Light Modulators*, vol. SL30. Bellingham, WA, USA: SPIE Press, 2017.
[5] A. Forbes, A. Dudley, and M. McLaren, "Creation and detection of optical modes with spatial light modulators," *Adv. Opt. Photon.*, vol. 8, pp. 200–227, Jun. 2016.
[6] D. J. Richardson, J. M. Fini, and L. E. Nelson, "Space-division multiplexing in optical fibres," *Nature Photon.*, vol. 7, pp. 354–362, Apr. 2013.
[7] S. Berdagué and P. Facq, "Mode division multiplexing in optical fibers.," *Appl. Opt.*, vol. 21, no. 11, pp. 1950–1955, 1982.
[8] G. Gibson *et al.*, "Free-space information transfer using light beams carrying orbital angular momentum," *Opt. Express*, vol. 12, no. 22, pp. 5448–5456, 2004.
[9] G. Keiser, *Optical Fiber Communications*. (McGraw-Hill Series in Electrical and Computer Engineering: Communications and Signal Processing), 3rd ed. New York, NY, USA: McGraw-Hill, 2000.
[10] J. Wang *et al.*, "Terabit free-space data transmission employing orbital angular momentum multiplexing," *Nature Photon.*, vol. 6, no. 7, pp. 488–496, 2012.
[11] V. Sleiffer *et al.*, "737 Tb/s ($96 \times 3\times$ 256-Gb/s) mode-division-multiplexed DP-16QAM transmission with inline MM-EDFA," *Opt. Express*, vol. 20, pp. B428–B438, Dec. 2012.
[12] H. Huang *et al.*, "100 Tbit/s free-space data link enabled by three-dimensional multiplexing of orbital angular momentum, polarization, and wavelength," *Opt. Lett.*, vol. 39, pp. 197–200, Jan. 2014.
[13] Y. Yan *et al.*, "High-capacity millimetre-wave communications with orbital angular momentum multiplexing," *Nature Commun.*, vol. 5, Sep. 2014, Art. no. 4876.
[14] M. Krenn *et al.*, "Communication with spatially modulated light through turbulent air across Vienna," *New J. Phys.*, vol. 16, no. 11, 2014, Art. no. 113028.
[15] A. Wang, L. Zhu, J. Liu, C. Du, Q. Mo, and J. Wang, "Demonstration of hybrid orbital angular momentum multiplexing and time-division multiplexing passive optical network," *Opt. Express*, vol. 23, pp. 29457–29466, Nov. 2015.
[16] Y. Ren *et al.*, "Experimental characterization of a 400 Gbit/s orbital angular momentum multiplexed free-space optical link over 120 m," *Opt. Lett.*, vol. 41, pp. 622–625, Feb. 2016.
[17] G. Xie *et al.*, "Experimental demonstration of a 200-Gbit/s free-space optical link by multiplexing Laguerre–Gaussian beams with different radial indices," *Opt. Lett.*, vol. 41, pp. 3447–3450, Aug. 2016.
[18] J. Wang, "Advances in communications using optical vortices," *Photon. Res.*, vol. 4, pp. B14–B28, Oct. 2016.
[19] N. Bozinovic *et al.*, "Terabit-scale orbital angular momentum mode division multiplexing in fibers," *Science*, vol. 340, no. 6140, pp. 1545–1548, 2013.
[20] H. Hübel *et al.*, "High-fidelity transmission of polarization encoded qubits from an entangled source over 100 km of fiber," *Opt. Express*, vol. 15, no. 12, pp. 7853–7862, 2007.
[21] R. Ursin *et al.*, "Entanglement-based quantum communication over 144 km," *Nature Phys.*, vol. 3, pp. 481–486, Jul. 2007.
[22] X.-S. Ma *et al.*, "Quantum teleportation over 143 kilometres using active feed-forward," *Nature*, vol. 489, no. 7415, pp. 269–273, 2012.
[23] T. Herbst, T. Scheidl, M. Fink, J. Handsteiner, B. Wittmann, R. Ursin, and A. Zeilinger, "Teleportation of entanglement over 143 km," *Proc. Nat. Acad. Sci. USA*, vol. 112, no. 46, pp. 14202–14205, 2015.

[24] T. Jennewein, C. Simon, G. Weihs, H. Weinfurter, and A. Zeilinger, "Quantum cryptography with entangled photons," *Phys. Rev. Lett.*, vol. 84, no. 20, pp. 4729–4732, 2000.

[25] A. Poppe *et al.*, "Practical quantum key distribution with polarization entangled photons," *Opt. Express*, vol. 12, no. 16, pp. 3865–3871, 2004.

[26] C.-Z. Peng *et al.*, "Experimental long-distance decoy-state quantum key distribution based on polarization encoding," *Phys. Rev. Lett.*, vol. 98, Jan. 2007, Art. no. 010505.

[27] J. Yin *et al.*, "Satellite-based entanglement distribution over 1200 kilometers," *Science*, vol. 356, no. 6343, pp. 1140–1144, 2017.

[28] H. Bechmann-Pasquinucci and W. Tittel, "Quantum cryptography using larger alphabets," *Phys. Rev. A*, vol. 61, May 2000, Art. no. 062308.

[29] N. J. Cerf, M. Bourennane, A. Karlsson, and N. Gisin, "Security of quantum key distribution using d-level systems," *Phys. Rev. Lett.*, vol. 88, Mar. 2002, Art. no. 127902.

[30] L. Sheridan and V. Scarani, "Security proof for quantum key distribution using qudit systems," *Phys. Rev. A*, vol. 82, Sep. 2010, Art. no. 030301.

[31] S. Gröblacher, T. Jennewein, A. Vaziri, G. Weihs, and A. Zeilinger, "Experimental quantum cryptography with qutrits," *New J. Phys.*, vol. 8, pp. 75–83, May 2006.

[32] M. Mafu *et al.*, "Higher-dimensional orbital-angular-momentum-based quantum key distribution with mutually unbiased bases," *Phys. Rev. A*, vol. 88, Sep. 2013, Art. no. 032305.

[33] M. Mirhosseini *et al.*, "High-dimensional quantum cryptography with twisted light," *New J. Phys.*, vol. 17, Mar. 2015, Art. no. 033033.

[34] B. Ndagano *et al.*, "Characterizing quantum channels with non-separable states of classical light," *Nature Phys.*, vol. 13, pp. 397–402, Jan. 2017.

[35] M. Krenn, M. Malik, M. Erhard, and A. Zeilinger, "Orbital angular momentum of photons and the entanglement of Laguerre–Gaussian modes," *Philos. Trans. Roy. Soc. Lond. A, Math. Phys. Eng. Sci.*, vol. 375, no. 2087, 2017, Art. no. 20150442.

[36] B. Ndagano *et al.*, "A deterministic detector for vector vortex states," *Sci. Rep.*, vol. 7, 2017, Art. no. 13882.

[37] A. Sit *et al.*, "High-dimensional intracity quantum cryptography with structured photons," *Optica*, vol. 4, pp. 1006–1010, Sep. 2017.

[38] M. McLaren, T. Konrad, and A. Forbes, "Measuring the nonseparability of vector vortex beams," *Phys. Rev. A*, vol. 92, no. 2, 2015, Art. no. 023833.

[39] Q. Zhan, "Cylindrical vector beams: From mathematical concepts to applications," *Adv. Opt. Photon.*, vol. 1, pp. 1–57, Jan. 2009.

[40] M. P. J. Lavery *et al.*, "Space division multiplexing in a basis of vector modes," in *Proc. Eur. Conf. Opt. Commun.*, Sep. 2014, pp. 1–3.

[41] J. Zhang, F. Li, J. Li, Y. Feng, and Z. Li, "120 Gbit/s 2 × 2 vector-modes-division- multiplexing DD-OFDM-32QAM free-space transmission," *IEEE Photon. J.*, vol. 8, no. 6, Dec. 2016, Art. no. 7907008.

[42] Y. Zhao and J. Wang, "High-base vector beam encoding/decoding for visible-light communications," *Opt. Lett.*, vol. 40, pp. 4843–4846, Nov. 2015.

[43] G. Milione *et al.*, "4 20 Gbit/s mode division multiplexing over free space using vector modes and a q-plate mode (de)multiplexer," *Opt. Lett.*, vol. 40, no. 9, pp. 1980–1983, 2015.

[44] G. Milione, T. A. Nguyen, J. Leach, D. A. Nolan, and R. R. Alfano, "Using the nonseparability of vector beams to encode information for optical communication," *Opt. Lett.*, vol. 40, pp. 4887–4890, Nov. 2015.

[45] P. Li, B. Wang, and X. Zhang, "High-dimensional encoding based on classical nonseparability," *Opt. Lett.*, vol. 24, pp. 15143–15159, Jun. 2016.

[46] B. Ndagano, R. Brüning, M. McLaren, M. Duparré, and A. Forbes, "Fiber propagation of vector modes," *Opt. Express*, vol. 23, pp. 17330–17336, Jun. 2015.

[47] P. Gregg *et al.*, "Q-plates as higher order polarization controllers for orbital angular momentum modes of fiber," *Opt. Lett.*, vol. 40, pp. 1729–1732, Apr. 2015.

[48] C. E. R. Souza, C. V. S. Borges, A. Z. Khoury, J. A. O. Huguenin, L. Aolita, and S. P. Walborn, "Quantum key distribution without a shared reference frame," *Phys. Rev. A*, vol. 77, Mar. 2008, Art. no. 032345.

[49] G. Vallone *et al.*, "Free-space quantum key distribution by rotation-invariant twisted photons," *Phys. Rev. Lett.*, vol. 113, Aug. 2014, Art. no. 060503.

[50] G. Milione, H. I. Sztul, D. A. Nolan, and R. R. Alfano, "Higher-order poincaré sphere, stokes parameters, and the angular momentum of light," *Phys. Rev. Lett.*, vol. 107, Jul. 2011, Art. no. 053601.

[51] M. J. Padgett and J. Courtial, "Poincaré-sphere equivalent for light beams containing orbital angular momentum," *Opt. Lett.*, vol. 24, pp. 430–432, Apr. 1999.

[52] A. Dudley, Y. Li, T. Mhlanga, M. Escuti, and A. Forbes, "Generating and measuring nondiffracting vector Bessel beams," *Opt. Lett.*, vol. 38, pp. 3429–3432, Sep. 2013.

[53] R. Brüning *et al.*, "Data transmission with twisted light through a free-space to fiber optical communication link," *J. Opt.*, vol. 18, no. 3, 2016, Art. no. 03LT01.

[54] B. Sephton, A. Dudley, and A. Forbes, "Revealing the radial modes in vortex beams," *Appl. Opt.*, vol. 55, no. 28, pp. 7830–7835, 2016.

[55] R. J. C. Spreeuw, "A classical analogy of entanglement," *Found. Phys.*, vol. 28, pp. 361–374, 1998.

[56] L. J. Pereira, A. Z. Khoury, and K. Dechoum, "Quantum and classical separability of spin-orbit laser modes," *Phys. Rev. A*, vol. 90, Nov. 2014, Art. no. 053842.

[57] F. Töppel, A. Aiello, C. Marquardt, E. Giacobino, and G. Leuchs, "Classical entanglement in polarization metrology," *New J. Phys.*, vol. 16, Jul. 2014, Art. no. 073019.

[58] D. Guzman-Silva *et al.*, "Demonstration of local teleportation using classical entanglement," *Laser Photon. Rev.*, vol. 10, no. 2, pp. 317–321, Jan. 2016.

[59] E. Karimi and R. W. Boyd, "Classical entanglement?" *Science*, vol. 350, pp. 1172–1173, Dec. 2015.

[60] E. Karimi *et al.*, "Spin-orbit hybrid entanglement of photons and quantum contextuality," *Phys. Rev. A*, vol. 82, Aug. 2010, Art. no. 022115.

[61] V. D'Ambrosio *et al.*, "Photonic polarization gears for ultra-sensitive angular measurements," *Nature Commun.*, vol. 4, Sep. 2013, Art. no. 2432.

[62] Y. Bromberg, Y. Lahini, R. Morandotti, and Y. Silberberg, "Quantum and classical correlations in waveguide Lattices," *Phys. Rev. Lett.*, vol. 102, Jun. 2009, Art. no. 253904.

[63] R. Keil, A. Szameit, F. Dreisow, M. Heinrich, S. Nolte, and A. Tünnermann, "Photon correlations in two-dimensional waveguide arrays and their classical estimate," *Phys. Rev. A*, vol. 81, Feb. 2010, Art. no. 023834.

[64] R. Keil, F. Dreisow, M. Heinrich, A. Tünnermann, S. Nolte, and A. Szameit, "Classical characterization of biphoton correlation in waveguide lattices," *Phys. Rev. A*, vol. 83, Jan. 2011, Art. no. 013808.

[65] G. M. Lerman, L. Stern, and U. Levy, "Generation and tight focusing of hybridly polarized vector beams," *Opt. Express*, vol. 18, no. 26, pp. 27650–27657, 2010.

[66] M. Michihata, T. Hayashi, and Y. Takaya, "Measurement of axial and transverse trapping stiffness of optical tweezers in air using a radially polarized beam," *Appl. Opt.*, vol. 48, no. 32, pp. 6143–6151, 2009.

[67] S. Berg-Johansen *et al.*, "Classically entangled optical beams for high-speed kinematic sensing," *Optica*, vol. 2, no. 10, pp. 1–5, 2015.

[68] A. Forbes, "Controlling light's helicity at the source: Orbital angular momentum states from lasers," *Philos. Trans. Roy. Soc. A*, vol. 375, no. 2087, 2017, Art. no. 20150436.

[69] D. Naidoo *et al.*, "Controlled generation of higher-order Poincaré sphere beams from a laser," *Nature Photon.*, vol. 10, pp. 327–332, Mar. 2016.

[70] S. Iwahashi, Y. Kurosaka, K. Sakai, K. Kitamura, N. Takayama, and S. Noda, "Higher-order vector beams produced by photonic-crystal lasers," *Opt. Express*, vol. 19, no. 13, pp. 119163–119168, 2011.

[71] X. Cai *et al.*, "Integrated compact optical vortex beam emitters," *Science*, vol. 338, pp. 363–366, Oct. 2012.

[72] K. A.-A. Darryl Naidoo, M. Fromager, and A. Forbes, "Radially polarized cylindrical vector beams from a monolithic microchip laser," *Opt. Eng.*, vol. 54, 2015, Art. no. 111304.

[73] W. Shu *et al.*, "Propagation model for vector beams generated by metasurfaces," *Opt. Express*, vol. 24, no. 18, pp. 21177–21189, 2016.

[74] P. Miao *et al.*, "Orbital angular momentum microlaser," *Science*, vol. 353, pp. 464–467, Jul. 2016.

[75] L. Gong *et al.*, "Generation of cylindrically polarized vector vortex beams with digital micromirror device," *J. Appl. Phys.*, vol. 116, no. 18, 2014, Art. no. 183105.

[76] Y.-X. Ren, Z.-X. Fang, L. Gong, K. Huang, Y. Chen, and R.-D. Lu, "Digital generation and control of Hermite–Gaussian modes with an amplitude digital micromirror device," *J. Opt.*, vol. 17, Dec. 2015, Art. no. 125604.

[77] M. A. A. Neil, F. Massoumian, R. Juskaitis, and T. Wilson, "Method for the generation of arbitrary complex vector wave fronts," *Opt. Lett.*, vol. 27, no. 21, pp. 1929–1931, 2002.

[78] C. Maurer, A. Jesacher, S. Fürhapter, S. Bernet, and M. Ritsch-Marte, "Tailoring of arbitrary optical vector beams," *New J. Phys.*, vol. 9, 2007, Art. no. 78.
[79] I. Moreno, J. A. Davis, T. M. Hernandez, D. M. Cottrell, and D. Sand, "Complete polarization control of light from a liquid crystal spatial light modulator," *Opt. Express*, vol. 20, no. 1, pp. 364–376, 2012.
[80] S. Pancharatnam, "Generalized theory of interference and its applications. Partially coherent pencils," *Proc. Indian Acad. Sci., Sect. A*, vol. 44, pp. 247–262, 1956.
[81] M. V. Berry, "Quantal phase factors accompanying adiabatic changes," *Proc. Roy. Soc. Lond. A, Math. Phys. Eng. Sci.*, vol. 392, no. 1802, pp. 45–57, 1984.
[82] E. J. Galvez, P. R. Crawford, H. I. Sztul, M. J. Pysher, P. J. Haglin, and R. E. Williams, "Geometric phase associated with mode transformations of optical beams bearing orbital angular momentum," *Phys. Rev. Lett.*, vol. 90, May 2003, Art. no. 203901.
[83] L. Marrucci, C. Manzo, and D. Paparo, "Optical spin-to-orbital angular momentum conversion in inhomogeneous anisotropic media," *Phys. Rev. Lett.*, vol. 96, Apr. 2006, Art. no. 163905.
[84] L. Marrucci *et al.*, "Spin-to-orbital conversion of the angular momentum of light and its classical and quantum applications," *J. Opt.*, vol. 13, Jun. 2011, Art. no. 064001.
[85] Z. Bomzon, V. Kleiner, and E. Hasman, "Pancharatnam–Berry phase in space-variant polarization-state manipulations with subwavelength gratings," *Opt. Lett.*, vol. 26, no. 18, pp. 1424–1426, 2001.
[86] Z. Bomzon, G. Biener, V. Kleiner, and E. Hasman, "Space-variant Pancharatnam–Berry phase optical elements with computer-generated subwavelength gratings," *Opt. Lett.*, vol. 27, no. 13, pp. 1141–1143, 2002.
[87] G. Biener, A. Niv, V. Kleiner, and E. Hasman, "Formation of helical beams by use of Pancharatnam–Berry phase optical elements," *Opt. Lett.*, vol. 27, pp. 1875–1857, Nov. 2002.
[88] E. Hasman, V. Kleiner, G. Biener, and A. Niv, "Polarization dependent focusing lens by use of quantized Pancharatnam-Berry phase diffractive optics," *Appl. Phys. Lett.*, vol. 82, no. 3, pp. 328–330, 2003.
[89] A. Niv, G. Biener, V. Kleiner, and E. Hasman, "Spiral phase elements obtained by use of discrete space-variant subwavelength gratings," *Opt. Commun.*, vol. 251, pp. 306–314, Jul. 2005.
[90] R. C. Devlin *et al.*, "Spin-to-orbital angular momentum conversion in dielectric metasurfaces," *Opt. Express*, vol. 25, no. 1, pp. 377–393, 2017.
[91] Z. Zhao, J. Wang, S. Li, and A. E. Willner, "Metamaterials-based broadband generation of orbital angular momentum carrying vector beams," *Opt. Lett.*, vol. 38, pp. 932–934, Mar. 2013.
[92] X. Yi *et al.*, "Generation of cylindrical vector vortex beams by two cascaded metasurfaces," *Opt. Express*, vol. 22, pp. 17207–17215, Jul. 2014.
[93] F. Yue, D. Wen, J. Xin, B. D. Gerardot, J. Li, and X. Chen, "Vector vortex beam generation with a single plasmonic metasurface," *ACS Photon.*, vol. 3, pp. 1558–1563, Sep. 2016.
[94] B. Ndagano, H. Sroor, M. McLaren, C. Rosales-Guzmán, and A. Forbes, "Beam quality measure for vector beams," *Opt. Lett.*, vol. 41, pp. 3407–3410, Aug. 2016.
[95] T. Kaiser, D. Flamm, S. Schröter, and M. Duparré, "Complete modal decomposition for optical fibers using CGH-based correlation filters," *Opt. Express*, vol. 17, pp. 9347–9356, May 2009.
[96] C. Schulze, S. Ngcobo, M. Duparré, and A. Forbes, "Modal decomposition without a priori scale information," *Opt. Express*, vol. 20, no. 25, pp. 27866–27873, 2012.
[97] I. a. Litvin, A. Dudley, F. S. Roux, and A. Forbes, "Azimuthal decomposition with digital holograms," *Opt. Express*, vol. 20, no. 10, pp. 10996–11004, 2012.
[98] C. Schulze, D. Flamm, A. Dudley, A. Forbes, and M. Duparré, "Modal decomposition for measuring the orbital angular momentum density of light," *Proc. SPIE*, vol. 8637, Mar. 2013, Art. no. 863719.
[99] Y. Li, J. Kim, and M. J. Escuti, "Orbital angular momentum generation and mode transformation with high efficiency using forked polarization gratings," *Appl. Opt.*, vol. 51, no. 34, pp. 8236–8245, 2012.
[100] G. C. G. Berkhout, M. P. J. Lavery, J. Courtial, M. W. Beijersbergen, and M. J. Padgett, "Efficient sorting of orbital angular momentum states of light," *Phys. Rev. Lett.*, vol. 105, Oct. 2010, Art. no. 153601.
[101] R. Fickler, R. Lapkiewicz, M. Huber, M. P. Lavery, M. J. Padgett, and A. Zeilinger, "Interface between path and orbital angular momentum entanglement for high-dimensional photonic quantum information," *Nature Commun.*, vol. 5, Jul. 2014, Art. no. 4502.
[102] M. P. J. Lavery *et al.*, "Efficient measurement of an optical orbital-angular-momentum spectrum comprising more than 50 states," *New J. Phys.*, vol. 15, Jan. 2013, Art. no. 013024.
[103] A. Ferenczi and N. Lütkenhaus, "Symmetries in quantum key distribution and the connection between optimal attacks and optimal cloning," *Phys. Rev. A*, vol. 85, May 2012, Art. no. 052310.
[104] C. Paterson, "Atmospheric turbulence and orbital angular momentum of single photons for optical communication," *Phys. Rev. Lett.*, vol. 94, no. 15, 2005, Art. no. 153901.
[105] M. Malik *et al.*, "Influence of atmospheric turbulence on optical communications using orbital angular momentum for encoding," *Opt. Express*, vol. 20, no. 12, pp. 13195–13200, 2012.
[106] B. Rodenburg *et al.*, "Influence of atmospheric turbulence on states of light carrying orbital angular momentum," *Opt. Lett.*, vol. 37, no. 17, pp. 3735–3737, 2012.
[107] S. K. Goyal, A. H. Ibrahim, F. S. Roux, T. Konrad, and A. Forbes, "The effect of turbulence on entanglement-based free-space quantum key distribution with photonic orbital angular momentum," *J. Opt.*, vol. 18, no. 6, 2016, Art. no. 064002.
[108] C. Chen, H. Yang, S. Tong, and Y. Lou, "Changes in orbital-angular-momentum modes of a propagated vortex Gaussian beam through weak-to-strong atmospheric turbulence," *Opt. Express*, vol. 24, no. 7, pp. 6959–6975, 2016.
[109] W. Wootters, "Entanglement of formation and concurrence," *Quantum Inf. Comput.*, vol. 1, no. 1, pp. 27–44, 2001.
[110] L. C. Andrews and R. L. Phillips, *Laser Beam Propagation Through Random Media*, vol. 1, 2nd ed. Bellingham, WA, USA: SPIE, Sep. 2005.
[111] M. A. Cox, C. Rosales-Guzmán, M. P. J. Lavery, D. J. Versfeld, and A. Forbes, "On the resilience of scalar and vector vortex modes in turbulence," *Opt. Express*, vol. 24, no. 16, pp. 18105–18113, 2016.

Authors' biographies not available at the time of publication.